



The Challenges and Opportunities of High-Spin Mn(II) EPR and ENDOR

Peter E. Doan¹ · Alex Drena¹ · Ajay Sharma¹ · Brian M. Hoffman¹

Received: 17 June 2024 / Revised: 2 July 2024 / Accepted: 5 July 2024 /

Published online: 22 July 2024

© The Author(s), under exclusive licence to Springer-Verlag GmbH Austria, part of Springer Nature 2024

Abstract

We examine the electron paramagnetic resonance (EPR) and electron-nuclear double resonance (ENDOR) spectroscopy of three quite distinct high-spin Mn(II) systems and describe experimental techniques and methods of analysis that are useful in their study. We demonstrate that this $S=5/2$ metal center provides useful orientation-selection through the Zero-Field Splitting (ZFS) tensor that enables determination of a ^{13}C hyperfine-coupling tensor with extremely small hyperfine interaction. We also demonstrate that Mims suppression effects can be used in concert with orientation-selection to edit complex $^{1,2}\text{H}$ ENDOR patterns that can be produced by even a ‘simple’ center with a single Mn(II). We develop a perturbation-based approach to understanding second-order shifts in Mn(II) ENDOR responses that occur in systems with intermediate ZFS values, and show that these shifts can be used to estimate the values of the ZFS tensors.

1 Introduction

In the past decade, we found that applications of 35 GHz EPR /ENDOR (electron paramagnetic resonance/electron-nuclear double resonance) in studies of high-spin Mn(II) systems can provide detailed information about the Mn center itself *and* non-bonded nuclei at surprisingly large distance from the Mn. We have used both CW (continuous-wave) passage-mode as well as echo-detected pulsed EPR spectroscopies to measure the zero-field splitting parameters (ZFS) that are indicative of differential Mn(II) speciation in heterogeneous biological samples [1–3]. The absorption-like lineshapes available in these techniques accentuates the broader features from the EPR ZFS transitions not associated with the central six-line isotropic pattern that tends to dominate standard derivative-display EPR measurements. These studies have been combined with ENDOR and ESEEM

✉ Peter E. Doan
ped131@northwestern.edu

¹ Department of Chemistry, Northwestern University, Evanston, IL 60626, USA

studies to determine the immediate coordination sphere of the Mn(II) ion [1, 4]. In another set of studies that utilize ENDOR measurements, the unique spin-physics of the $S=5/2$ at high polarization (higher frequencies and low temperatures) gives rise to orientation-selection that is similar to those seen in simple $S=1/2$ systems with g -anisotropy. This provides access to highly resolved spectra that provide excellent geometric information concerning non-coordinated nuclei up to 5 Å from the central metal [3, 5, 6]. In so doing, we have obtained detailed information concerning substrate binding to lipoxxygenase enzymes and changes in the environment around the central metal ion.

There are comprehensive reviews [7, 8] of advanced magnetic resonance studies of manganese centers in biological systems that cover many of the opportunities. In addition, many of the challenges in the experimental protocols of the analyses of high electron spin systems such as Mn(II) and Gd(III) have been detailed by Astashkin and coworkers [9, 10] as well as by Stoll and Britt [11]. However, the growing incorporation of this metal ion into our work has led us to devise strategies that are purpose-built (ad hoc) rather than more general, and that at minimum give transparent explanations for a variety of otherwise puzzling observations. These techniques have been applied in a series of studies, in so doing detail the advantages and disadvantages of the processes described. Specifically, we describe: (1) Field-dependent orientation-selective determination of the full hyperfine tensor of a ^{13}C with remarkably small couplings (<0.3 MHz); (2) the use of Mims suppression effects to edit pulsed ENDOR data to verify assignments; (3) an explanation of second-order shifts in ENDOR frequencies that arise when the ZFS interaction is of ‘intermediate strength’, and that provide precise estimates of those parameters.

2 Background

2.1 First-Order Analysis: EPR

Many of the concepts discussed here have been demonstrated by Stoll and Britt [11] as well as Astashkin et al. [10] in their work on Gd(III). We begin by recapitulating their work before considering certain behaviors that were not anticipated in their analysis. The Hamiltonian for the terms that define the EPR of the $S=5/2$, $I=5/2$ Mn(II) ion in a weak ligand field is given in Eq. (1)

$$H_{\text{EPR}} = \underbrace{\left\{ \beta_e \left(\hat{S} \cdot g \cdot \vec{B} \right) + \left(\hat{S} \cdot \underline{D} \cdot \hat{S} \right) + h \left(\hat{S} \cdot \underline{A}^{(55}\text{Mn}) \cdot \hat{I}_{\text{Mn}} \right) \right\}}_{\{\text{EPR}\}} + \underbrace{\left\{ g_n \beta_n \hat{I}_n \cdot \vec{B} + \hat{S} \cdot \underline{A}_n \cdot \hat{I}_n \right\}}_{\{\text{ENDOR}\}} \quad (1)$$

For the systems we are examining the electron Zeeman interaction is effectively isotropic with $g \sim 2.00$ and the HFI of the $I=5/2$ ^{55}Mn nucleus is also effectively isotropic with hyperfine coupling of approximately $a(^{55}\text{Mn}) \approx 250$ MHz, leaving the

only major anisotropic term in the EPR spin Hamiltonian arising from the ZFS tensor. At 35 GHz, the magnitude of the electron Zeeman interaction is much greater than the ZFS terms and we can treat $|S, m_S\rangle$ and $|I, m_I\rangle$ for ^{55}Mn as good quantum number, and the first order energy levels can be written as

$$e(m_S, m_I; \theta, \phi) = 2\beta_e B m_S + m_S^2 D(\theta, \phi) + m_S m_I A_{Mn} \quad (2)$$

where $D(\theta, \phi)$ is the orientation-dependent ZFS interaction. The selection rules for EPR are $\Delta m_S = \pm 1$, $\Delta m_I = 0$, so an EPR spectrum contains six equally spaced $m_S \rightarrow m_S + 1$ transitions

$$\Delta e(m_S, m_I; \theta, \phi) = 2\beta_e B + (2m_S + 1)D(\theta, \phi) + m_I A_{Mn} \quad (3)$$

As any ENDOR transition not involving the ^{55}Mn nucleus itself, the ^{55}Mn HFI will simply act as an energy offset to any given EPR fine structure transition.

2.2 First-Order Analysis: ENDOR of Hyperfine-Coupled Nucleus

Our interest is in the ENDOR of hyperfine-coupled nuclei from Mn(II) ligands and adjacent entities. These couplings are invariably small so as not to be resolvable in an EPR spectrum and the contribution of such a nucleus to the spin-Hamiltonian energies can be written by adding simple first-order terms to the first-order perturbation levels of Eq. (1)

$$e(m_S, m_I) = m_I m_S A(\theta, \phi) + m_I \nu_N \quad (4)$$

where ν_N is the Larmor frequency of nucleus and the observing magnetic field, and $A(\theta, \phi)$ is the orientation-dependent hyperfine interaction. ENDOR transitions are tied to a specific EPR transition and, therefore, to a specific value of m_S , and for an $I = 1/2$ nucleus where $|\nu_N| > |A(\theta, \phi)|$, we can write the allowed ENDOR transitions

$$\begin{aligned} \nu_- &= |\nu_N - m_S A(\theta, \phi)| \\ \nu_+ &= |\nu_N - (m_S + 1)A(\theta, \phi)| \end{aligned} \quad (5)$$

Equation (5) predicts two peaks separated by $|A|$ and centered not at ν_N but at $\nu_N - (m_S + 1/2)A(\theta, \phi)$.

This provides two levels of orientation-selection in an ENDOR experiment. The first is an EPR-selection where the $D(\theta, \phi)$ will determine which of the fine-structure transitions giving its own response, and thus, independently essentially acting like one of a set of five different molecules. The second level involves the set of orientations in resonance for the nuclear HFI tensor(s) being studied; at a general observing field this is expected to be different for each of the fine-structure transitions.

3 Experimental

35 GHz CW EPR spectra were obtained at 2 K on a modified Varian E-110 that has been described [12]. Pulsed 35 GHz Echo-detected EPR (ED-EPR) and pulsed ENDOR [13] were obtained at 2 K on a locally-constructed spectrometer that has been described previously. Data acquisition software SpecMan4EPR [14] was used for all experiments. ED-EPR spectra were collected using either a 2-pulse (Hahn echo) sequence $t_{90}-\tau-t_{180}$ or a 3-pulse stimulated echo sequence $t_{90}-\tau-t_{90}-T-t_{90}-\tau$ -echo. Davies ENDOR, Mims ENDOR, Refocused Mims (reMims) used a 4-pulse echo sequence $t_{90}-\tau-t_{90}-T-t_{90}-\tau_1-t_{180}-(\tau+\tau_1)$ -echo. All ENDOR spectra were collected with random-hopping of the RF [15].

Simulations of EPR were obtained with EasySpin [16]. Simulations of ENDOR used either EasySpin or the locally-written software Bellagio described in the SI.

The samples of $\text{Mn}(\text{D}_2\text{O})_5(\text{Imidazole})$ examined here were prepared by diluting 20 μL of a concentrated aqueous buffer of 100 mM MOPS (3-(*N*-morpholino)propanesulfonic acid), 20 mM Imidazole (Im) at pH 7.0 into 200 μL of a solution containing 250 μM $\text{Mn}(\text{II})\text{Cl}_2$ dissolved in a 80:20 mixture of $\text{D}_2\text{O}:\text{d}_3$ -glycol. We review studies of a heteroscorpionate Mn^{2+} -hydride complex [17] and lipoxxygenase Mn^{2+} enzymes [3, 5, 6, 18] prepared as previously described.

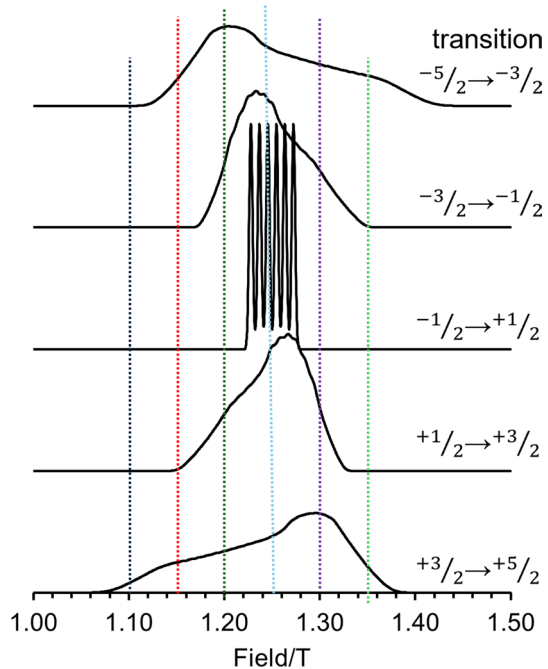
4 Analysis and Results

4.1 Fine-Structure Selection

For ENDOR analysis in Mn(II) systems, we examine the decomposition of the EPR spectrum into its component fine-structure transitions shown in Fig. 1. Each of the separate fine-structure transition looks like a simple $S = 1/2$ center with highly anisotropic g -tensor, except for the transition from $m_s - 1/2 \rightarrow + 1/2$, which occurs without any first-order dependence on D and is therefore a powder-averaged pattern. At higher magnetic fields (microwave frequencies) and lower temperatures, the Boltzmann populations of the electron-spin energy levels (Eq. 2) become important in describing the appearance of both the EPR and ENDOR spectra. At 35 GHz ($B_C = 1.25$ T) and in superfluid liquid helium, nominally 2 K, the value of $h\nu_e/k_B T$ is 0.83 and the population differences of the fine-structure transitions drops by 43% for each +1 in m_s Eq. (2). ENDOR intensities are expected to be proportional to the intensities of their EPR transitions in any well-behaved system. For the same system at 10 K, the intensities would drop by only ~15% for each +1 change in m_s . The effects of the thermal depopulation on the appearance of the EPR spectrum has been discussed previously [5].

To demonstrate the ways in the fine structure selection affects the observed ENDOR pattern we use an isotropic hyperfine coupling to focus on the EPR orientation dependence and eliminate the complexity of the NMR orientation dependence, considering ^1H ENDOR with $A = a_{\text{iso}} = -2.0$ MHz. The patterns for

Fig. 1 Simulated of EPR fine structure transitions as separate components to illustrate the effects of both fine structure selection and orientation selection. Each of the separate transitions can be analyzed separately but the resulting ENDOR spectrum will be a weighted sum of the contributions. The intensities are scaled for display and not reflective of contribution to EPR absorption envelope. The colored vertical lines are the field positions used for ENDOR simulation in Fig. 2



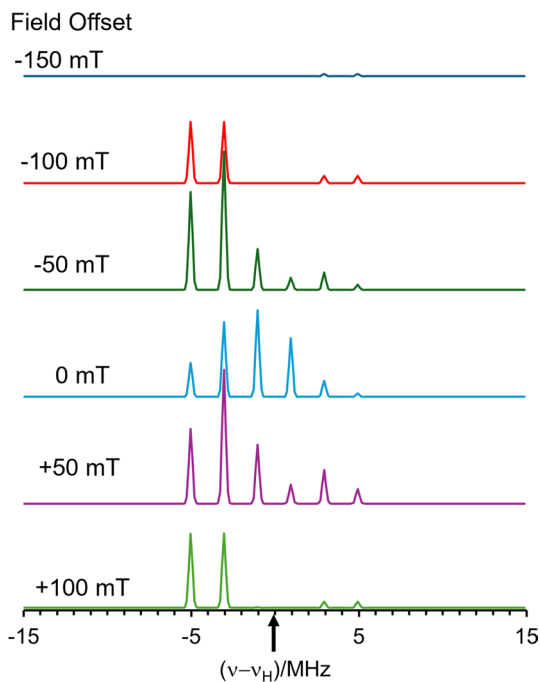
an Mn(II) with zero-field splitting tensor $D = (-300, -700, +1000)$ MHz with distribution in values $\Delta D = (30, 70, 100)$ MHz, $g = 2.0$ and thus Q-band center-field of $B_c = 1.25$ T are shown in Fig. 2. Considering the ENDOR responses predicted as the observing field is moved across the EPR envelope, for the isotropic hyperfine of $|2 \text{ MHz}|$ Eq. (5) shows that a simulation will give a regular pattern with 2 MHz splittings of doublet peak frequencies, with offsets from the ^1H Larmor frequencies running from -5 to $+5$ MHz as m_s successively interrogates fine-structure EPR transitions from -2.5 to $+2.5$. The only variable is the intensity as controlled by the contribution of the fine-structure transition to the EPR intensity at a given field offset, with the intensities of the resulting five different ENDOR spectra (one per fine structure transition) weighted by their Boltzmann populations at 2 K and summed.

At -150 mT , the lowest field offset, the $+3/2 \rightarrow +5/2$ transition would contribute a response that would be near a 'Z' direction turning point, but this is the transition between the two highest energy levels and at 2 K, these levels are highly depopulated—hence, no ENDOR signal.

At -100 mT , the EPR envelope at this field has its dominant contribution from the $-5/2 \rightarrow -3/2$ transition and the ENDOR shows two lines of equal intensity at -5 MHz, and -3 MHz from the Larmor frequency. As these are the two lowest energy levels, their population difference is the largest.

At -50 mT , there is a small the between the two has the which arise from the two lowest energy levels. There are small intensity peaks from two higher lying EPR transitions, the $+1/2 \rightarrow +3/2$ and $+3/2 \rightarrow +5/2$ at frequency offsets $+1, +3, +5$ MHz.

Fig. 2 Simulation of ENDOR spectrum across EPR envelope of a hypothetical Mn(II) EPR center shown Fig. 1 and an isotropic proton with $A = -2.0$ MHz. 5 orientation-dependent ENDOR patterns are weighted by Boltzmann factors assuming a temperature of 2 K. EPR parameters as in Fig. 1 with the exception of $A(^{55}\text{Mn})$. Instead, a window of ± 25 mT was used in the program Bellagio to simulate the influence of the ^{55}Mn HFI



These are heavily depopulated due the low temperatures. As the field is increased to an offset of -100 mT, we see a small contribution at -1 MHz that arises from some population of the $-3/2 \rightarrow -1/2$ fine structure transition, so effectively all 6 possible ENDOR transitions are observed.

By -50 mT, there are small contributions to the ENDOR spectrum from the $-3/2 \rightarrow -1/2$ (-3 MHz, -1 MHz) as well as the $(+1/2 \rightarrow +3/2)$ (+1 MHz, +3 MHz) significant contributions from the $-3/2 \rightarrow -1/2$ fine structure transition, so the peak at -3 MHz now represents the sum of two separate EPR transitions.

At B_C , the central field value, the ENDOR pattern is dominated by the peaks at ± 1 MHz. Though the major contribution to this set of peaks is from the $-1/2 \rightarrow +1/2$ fine structure transition, simply examining the spectrum at -50 and +50 mT shows that significant portions of these intensities are associated with the other EPR transitions.

By +50 mT above B_C , the contribution from the $-3/2 \rightarrow -1/2$ fine structure transition has dropped to approximately 50% of the contribution from the $-5/2 \rightarrow -3/2$ fine structure transition. The lower-intensity peaks above the Larmor frequency arise from the higher lying energy levels and would be difficult to observe in an actual experiment.

By +100 mT, the only observable ENDOR transitions are associated with the lowest energy EPR doublet. This highest field represents the 'Z' direction of the ZFS tensor for this manifold.

The breaking down of the ENDOR into its different components can simplify analysis of orientation selection as it isolates the particular set of orientations

that are expected at any given observing field position. The ENDOR transitions associated with the $m_s = \pm 1/2$ EPR states can only be observed outside of the central region when the $-3/2 \rightarrow -1/2$ or $+1/2 \rightarrow +3/2$ transitions make up a significant fraction of the EPR signal. The appearance of new lines in the ENDOR spectrum as the field is changed can then be used as a method of more precisely defining the ZFS parameters.

4.2 Orientation-Selective Analysis with Small Hyperfine Couplings

One of the major benefits of high-electron spin systems is that the hyperfine split doublets from different fine-structure transitions are not all centered at the Larmor frequency, but shifted by $m_s A$. This accomplishes two very important tasks; first, it spreads out the frequencies and allows for more facile assignments peaks with manifolds; second, it separates peaks by hyperfine sign for the four EPR transitions that are sensitive to D . This is of crucial importance in studies involving weakly dipolar-coupled nuclei. We describe the position of the nucleus in terms of its polar coordinates (R, θ_n, ϕ_n) in the D -tensor axis system where we approximate the hyperfine interaction by

$$A = T(3 \cos^2 \eta - 1) + a_{iso} \quad (6)$$

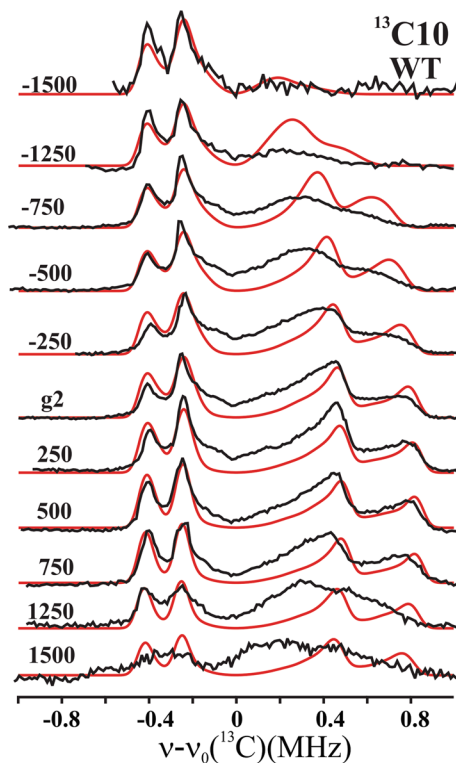
where $T = g_n \beta_n g_e \beta_e / R^3$ and η is the angle between the applied field vector and the metal-nucleus vector. There are three parameters we would like to extract from such ENDOR data: R , the distance between the metal center and the nucleus, a_{iso} , the isotropic hyperfine interaction, and the azimuthal angle θ from the molecular Z axis.

In any $S = 1/2$ systems with $a_{iso} \sim 0$, when $\eta = 0^\circ$, the ENDOR frequencies are $\nu_N \pm T$ and when $\eta = 90^\circ$, $\nu_N \pm T/2$. In a powder ENDOR pattern there is only a separation of $T/2$ between the parallel and perpendicular transitions. In many systems we study, this is on the order of the ENDOR linewidths. It is typically easy to observe the perpendicular T , as simply by statistical arguments, its intensity tends to dominate the appearance of the spectra, but it is often difficult to make precise confirming measurements on the parallel features. In contrast when measuring the response to the $m_s -5/2 \rightarrow -3/2$ fine structure transition in a Mn(II) system, with the same T , the frequencies for the perpendicular are ($\nu_N - 2.5 T$, $\nu_N - 1.5 T$) and for parallel ($\nu_N + 3 T$, $\nu_N + 5 T$). That is, rather than peak separation of $1/2 T$, we see peak separation in multiples of T .

An example of the advantages of the high electron spin system in studying weakly dipolar coupled nuclei comes from a recent study of a series of lipoxygenases with their natural substrate, linoleic acid (LA) selectively labeled with ^{13}C [3, 5, 6, 18]. The distances between the Mn center and the labeled nucleus were greater than 4.5 and at such extreme distances $T < 0.3$ MHz.

^{13}C Mims ENDOR spectra were collected across the entire EPR envelope of Mn^{2+} -substituted soybean lipoxygenase with $^{13}\text{C}10$ -labelled lipoic acid substrate [5], Fig. 3, and they were simulated with the simple point-dipole model of Eq. (6). The spectra are relatively simple, as they contain only ENDOR responses from the $-5/2 \rightarrow -3/2$ EPR transition. This is actually anomalous because, as discussed above,

Fig. 3 Field-dependent ^{13}C Mims ENDOR spectra (black) and simulation of $m_s = -5/2 \rightarrow m_s = -3/2$ (red) collected across EPR envelope for the system Mn-SLO (soybean lipoxygenase) with bound $^{13}\text{C}10$ lipoic acid (LA). Fields are given as offsets from $g = 2.00$ in kG. Experimental parameters: 34.80 GHz , $t_{90} = 50\text{ ns}$, $T_{\text{RF}} = 45\text{ }\mu\text{s}$, $t = 1.5\text{ }\mu\text{s}$, repetition rate 100 Hz , $T = 2\text{ K}$. Simulation parameters: $D = (-220, -660, 880)\text{ MHz}$, $DD = (25, 25, 50)\text{ MHz}$, $T = 0.17\text{ MHz}$, $\theta = 50^\circ$, $\phi = 0^\circ$, $LW = 50\text{ kHz}$



even at 2 K we would expect responses from other EPR transitions. The anomaly lies in the variation of the responses of the EPR transitions with τ , as discussed in SI.

The perpendicular turning points of the dipolar interaction are seen across the entire EPR envelope as the two peaks at $\sim(-0.4, -0.2)$. The parallel turning points at frequencies $\sim(+0.4, +0.75)$ are substantially broader and have their maximum observed A in the field region between -25 and $+25\text{ mT}$. As discussed in detail in the SI of reference [5], this implies that orientation of the dipolar vector lies near a set of orientations with $D_{\text{eff}} \sim 0$. Given D tensor values $(-220, -660, +880)\text{ MHz}$, we can quickly extract the θ value for when $D_{\text{eff}} = 0$ for the specific orientations of the field in the XZ and YZ planes.

$$\text{XZ : } \theta_X = \text{acos} \left[\left(\frac{-D_X}{D_Z - D_X} \right)^{\frac{1}{2}} \right] \quad \text{YZ : } \theta_Y = \text{acos} \left[\left(\frac{-D_Y}{D_Z - D_Y} \right)^{\frac{1}{2}} \right] \quad (7)$$

For this system, these two angles are $\theta_X = 63^\circ$ and $\theta_Y = 49^\circ$. We need only test these two extremes in our simulations using the value of T (or R) the perpendicular turning points. In this system, we found that this Mn-C(10) vector lies in the YZ plane of the ZFS tensor. The hyperfine tensors thus determined for a substrate

lipoic acid $^{13}\text{C}10$ in two conformations had dipolar symmetry with dipolar coupling parameters (T , Eq. 6) that corresponded to Mn- $^{13}\text{C}10$ distance of $R=4.84$ and 5.21 \AA , while distances for the actual enzymatic target $^{13}\text{C}11$ were $r=4.89$ and 5.65 \AA (!) [5].

4.3 Mims-Editing of ENDOR Spectra

In $S=1/2$, $I=1/2$ systems where $|A| < \nu_N$, the two ENDOR lines of an ENDOR doublet for a single orientation exhibit a frequency offset from the Larmor frequency of absolute magnitude $\Delta\nu = 1/2|A|$. Therefore, there is a simple 1:1 correspondence between frequency offset and $|A|$. Under these conditions, the Mims ENDOR intensity function $I(\tau, A) = \sin^2(\pi A\tau)$, τ in μs , A in MHz, which leads to what are often referred to as 'Mims holes' where the intensity of the ENDOR response goes to zero when $A\tau = n$, $n=0, \pm 1, \pm 2, \dots$, and this can be rewritten in terms of frequency offsets as $I(\tau, \Delta\nu) = \sin^2(\pi \Delta\nu\tau/2)$. Likewise, the intensity function predicts maxima at $A\tau = \pm 1/2, \pm 3/2, \dots$

In the $S=5/2$ case of Mn(II), the Mims intensity function with respect to A is unchanged but there is no longer a simple 1:1 correspondence between frequency offset and A . For example, with $A = +3 \text{ MHz}$, the ENDOR lines for the $m_S -5/2 \rightarrow -3/2$ EPR transition would give $\Delta\nu_{\pm} = 7.5, 4.5 \text{ MHz}$. These peaks would be suppressed with $\tau = 0.33 \mu\text{s}$. For the same EPR transition, an $A = +1.8 \text{ MHz}$ would have peaks at $\Delta\nu_{\pm} = 4.5, 2.7 \text{ MHz}$ and they would be near a maximum at $\tau = 0.33 \mu\text{s}$. This shows that a peak at 4.5 MHz would be both at a minimum and a maximum in the intensity function for two different A values. Peaks with different A values and Mims ENDOR response functions from more than one EPR transition can also overlap. This can create a complicated ENDOR pattern for even a single nucleus, giving rise to a forest of overlapping peaks. However, we can apply Mims ENDOR suppression effects [19] to edit ENDOR patterns to test possible assignments.

A simple test system for this work is the complex pentaquaamidazole Mn(II), $[\text{Mn}(\text{II})(\text{D}_2\text{O})_5\text{Im}]^{2+}$. Our interest in this particular system stems from the hope that we might be able to use ^1H ENDOR signatures from a histidine imidazole ligand to define a molecular geometry in the coordination sphere relative to the ZFS tensor directions. As such, this model complex shows well-resolved ENDOR peaks from a single non-exchangeable proton on the imidazole ligand. The Echo-Detected EPR (ED-EPR) using a simple 2-pulse (Hahn echo) is given in the SI. The D , E values are estimated at (3000,400) MHz or $D = (-600, -1400, +2000) \text{ MHz}$.

We acquired a Davies ENDOR spectrum at the peak of the EPR envelope ($B = 1.235\text{T} \sim B_C$) shown in Fig. 4. The spectrum shows multiple well-resolved peaks. There is set of narrower features at $-4.50, -2.62, -0.83, +0.96 \text{ MHz}$ as well as broader features at $+5.3$ and $+1.1 \text{ MHz}$. As we are measuring in the center of the pattern, the ENDOR will show major contributions from each of the fine structure transitions: $-5/2 \rightarrow -3/2$, $-3/2 \rightarrow -1/2$ and $-1/2 \rightarrow +1/2$. Assuming a point-dipole hyperfine tensor for this H(Im), we assign the set of narrow peaks at $-4.5, -2.62, -0.83$ and $+0.96$ as perpendicular ENDOR features for the EPR manifolds ($-5/2, -3/2, -1/2, +1/2$) respectively, which gives a value of $A_{\perp} \sim -1.8 \text{ MHz}$. In a

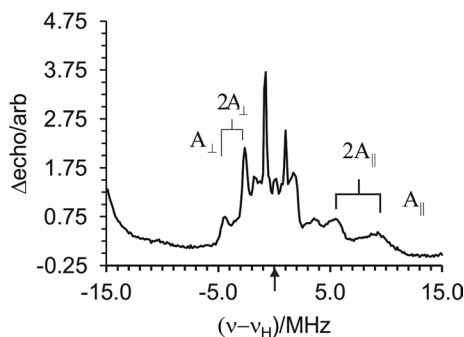


Fig. 4 ^1H Davies ENDOR spectrum of $\text{Mn}(\text{D}_2\text{O})_5(\text{Im})^{2+}$. ENDOR spectrum. The spectrum is a sum of the responses from multiple EPR transitions. The sharper lines below the Larmor frequency are assigned to perpendicular turning points, the broader peaks above the Larmor frequency are assigned to parallel turning points as shown in the annotation. Experimental conditions: t_{90} 60 ns, t_{180} 120 ns, $\tau=600$ ns, $T_{\text{RF}}=25$ us, repetition rate 100 Hz, temperature 2 K

similar fashion, the ENDOR peaks at (+5.3, +9.1) can be tentatively assigned to the $-5/2 \rightarrow -3/2$ fine structure transition with an A value of approximately +3.6 MHz. Spectra taken across the EPR envelope appear to confirm this assignment (data shown in SI). We note that this is the type of complexity in the ENDOR spectroscopy that we expected in the study of ^{13}C substrates described above.

We can easily test these assignments by using Mims ENDOR and selectively editing to suppress peaks as shown in Fig. 5. We used a refocused Mims (reMims) ENDOR sequence to allow for the short τ of 0.120 μs . The reMims ENDOR spectrum with $t=0.120$ μs is effectively identical to the Davies ENDOR spectrum shown in Fig. 4. None of the major peaks exhibit any significant changes in intensity relative to the Davies ENDOR spectrum. When the τ is changed to 0.250 μs , the peaks

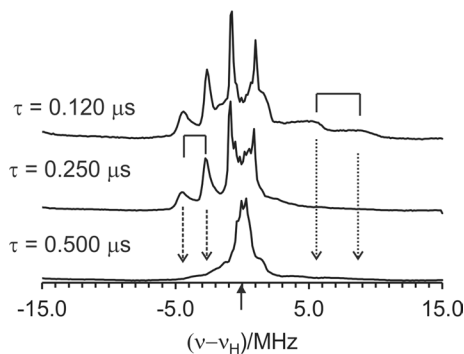


Fig. 5 Refocused Mims ENDOR collected at the same field position in Fig. 2. Using $\tau=0.120$ ns (top) the entire ENDOR spectrum is nearly identical to the Davies ENDOR spectrum in Fig. 2. Setting $\tau=0.250$ μs , (middle) the outer peaks in the + region are suppressed as it expected for $|A| \sim 4$ MHz. Setting $\tau=0.500$ μs , all of the resolved ENDOR features are abolished. Experimental conditions: $t_{90}=25$ ns, $t_{180}=50$ ns, $t_1=550$ ns, $T_{\text{RF}}=25$ us, repetition rate 100 Hz, 2 K

above the Larmor frequency are suppressed, showing that these peaks arise from $|A_{\parallel}|$ values of approximately 4 MHz. The small shoulder to the high frequency side of the central lines is also suppressed. This feature is likely due to the parallel orientation in the $-1/2 \rightarrow +1/2$ transition. In the lowest spectrum, when $\tau=0.500$ ns, the entire set of narrow lines is suppressed, as is expected for $|A_{\perp}| \sim 2$ MHz.

4.4 [4.4] 'Intermediate ZFS': ZFS-Induced Spin State Mixing Visible by ENDOR Spectroscopy

The equations derived for the ENDOR peaks Eq. (5) are a result of treating the ZFS interaction as a first-order perturbation on the electron Zeeman interaction. This approach is appropriate when the ZFS is quite small compared to the Zeeman interaction, and m_s , therefore, can be considered a 'good quantum number'. In the opposite 'large' ZFS regime, where the ZFS are much greater than the Zeeman interaction, EPR transitions involve the lowest lying sublevels, usually $m_S = \pm 1/2$. However, we have encountered an 'intermediate' ZFS regime, the ZFS terms are less than the Zeeman interaction, but are sufficiently strong as to require the incorporation of first order mixing of m_s states by the ZFS interaction. As reviewed here, this case is exhibited by a high-spin Mn^{2+} hydride/deuteride (Mn-H/D), where such a ZFS impacts $^1\text{H}/^2\text{H}$ ENDOR spectroscopy.

Figure 6 shows the 2 K 35 GHz CW EPR spectrum of the recently studied heteroscorpionate Mn-H complex [17]. The ZFS is a substantial fraction of the electron Zeeman interaction, as shown by the simulation using EasySpin with ZFS

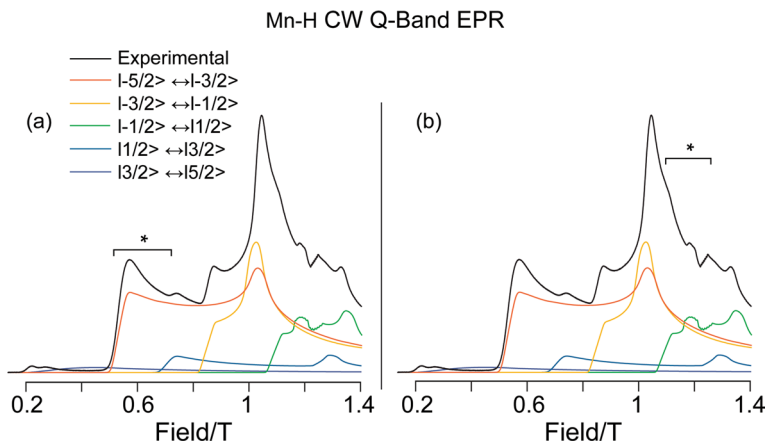


Fig. 6 2 K 35 GHz absorption-display CW EPR spectra of Mn-H (black trace) with simulated contributions from individual transitions differentiated by color. Microwave frequency: 34.874 GHz; power attenuation: 20 dB; modulation: 1.6 G; time constant: 64 ms. Parameters used for simulation are $D=7600$ MHz; $E/D=0.15$; $A=250$ MHz; $f=0.05$, $g=2.0$. Asterisk marked brackets denoted field ranges observed experimentally, corresponding to the low-field edge of the EPR spectrum with orientations in which the Y -axis of the ZFS tensor is aligned with the external magnetic field for the $-5/2 \rightarrow -3/2$ manifold (a), and where contributions include the central $-1/2 \rightarrow +1/2$ manifold (b)

parameters $D=7600$ MHz and $E/D=0.15$; the contributions from each sublevel transition manifold are shown individually, as well. The two bracketed regions in both Fig. 6a, b signify magnetic field ranges studied by ENDOR spectroscopy. Here, we discuss (a) measurements at fields along the low-field edge of the EPR spectrum, which are associated only with the $-5/2 \rightarrow -3/2$ manifold; measurements covering (b) a region near $g=2.0$ (1.25 T at 35 GHz) which includes significant contribution from the central $-1/2 \rightarrow +1/2$ transition, also have been reported [17].

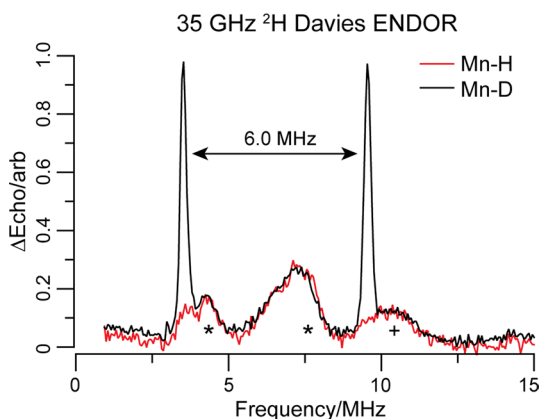
^2H ENDOR at the very low-field edge of the EPR spectrum of Mn–D yields single-crystal-like spectra for molecules oriented so that the external field lies along the Y -axis of the ZFS D -tensor (Fig. 7). The sharp peaks in Mn–D were confirmed as a hyperfine-split ^2H doublet by observing the τ -dependent behavior of the ENDOR response by the Mims pulse sequence.

However, if we assigned A in Eq. (5) as the doublet splitting, the center-frequency of the doublet does not fall at $|\nu_N + 2A|$, as required by Eq. (5). As now discussed, this discrepancy reveals that Eq. (5) does not quantitatively describe the behavior of the Mn–H/D complex, that the difference between the peak frequency gives only an *apparent* hyperfine splitting, and that Eq. (5) must be extended to incorporate ZFS-induced mixing of m_s sublevels. This analysis leads to an ENDOR response that still can be described by equations of precisely the *form* of Eq. (5), still using half-integer ' m_s ' constants, $-5/2, -3/2$, etc. while the sublevel mixing is accounted for by incorporating an *effective* hyperfine coupling, A_B' , that is *defined* by the observed differences in the peak frequencies of an ENDOR ν_+/ν_- doublet ($\Delta\nu_{\text{obs}}$), Eq. (8).

$$\Delta\nu_{\text{obs}} = |A_B'| \quad (8)$$

To understand this 'intermediate ZFS' regime, where the 'small-ZFS' Eq. (5), are inaccurate but the 'large-ZFS' regime, is not approached, we developed the perturbation theory treatment presented below, showing how sublevel mixing alters the ENDOR doublet splitting from the intrinsic coupling associated with the electron-nuclear spin Hamiltonian, A_B , with an attendant shift of the center-frequency of the doublet. This mixing can be quenched by using higher microwave frequencies and higher magnetic fields [20].

Fig. 7 ^1H and ^2H Davies ENDOR for Mn–H (red trace) and Mn–D (black trace) at 0.535 T and 2 K. Microwave frequency: 34.6 GHz; microwave pulse length (π): 80 ns (^1H Davies), 200 ns (^2H Davies); τ : 600 ns; RF pulse length: 15 μs (^1H Davies), 60 μs (^2H Davies); repetition rate: 5 ms. Spectra intensities have been scaled arbitrarily for clarity



We begin by rewriting the Hamiltonian shown in Eq. (1), omitting the term for the manganese HFI,

$$\hat{H} = \hat{H}_0 + \hat{H}_1 + \hat{H}_2 \tag{9}$$

where

$$\hat{H}_0 = 2\beta_e \hat{S} \cdot \vec{B} \tag{10a}$$

$$\hat{H}_1 = D_X \hat{S}_X^2 + D_Y \hat{S}_Y^2 + D_Z \hat{S}_Z^2 \tag{10b}$$

$$\hat{H}_2 = \hat{S} \cdot A \cdot \hat{I} + g_n \beta_n \hat{I} \cdot \vec{B} \tag{10c}$$

The electron Zeeman interaction, H_0 , is the largest and the electron spins quantize along the field.

$$H_0 |S, m_S\rangle = m_S g_e \beta_e B |S, m_S\rangle \tag{11}$$

We have developed this approach assuming the field is applied along the Y axis of the ZFS tensor, but can be generalized to the field along any of the canonical ZFS axes. Applying \hat{H}_1 to the eigenstates of \hat{H}_0 gives the first-order energy correction when the field is applied along the Y axis of the ZFS tensor,

$$e^{(1)} = m_S^2 D_Y \tag{12}$$

the same result as described in Eq. (2).

When the magnetic field is applied along the Y-direction of the D -tensor, the off-diagonal elements of the \hat{H}_1 matrix are given by

$$1/2 \epsilon \langle S, m_S | (\hat{S}_+^2 + \hat{S}_-^2) | S, m_S \pm 2 \rangle \tag{13}$$

where, with the field along Y,

$$\epsilon = \frac{1}{2} (D_Z - D_X) \tag{14}$$

First-order ZFS corrections to the $|S, m_S, n\rangle$ basis set in a magnetic field B gives the first-order-corrected wavefunctions for the six spin substates ψ_{1-6} as:

$$|\psi_6\rangle \approx \left| \frac{5}{2} \right\rangle - \frac{\sqrt{10}\epsilon}{4\beta_E B} \left| \frac{1}{2} \right\rangle \tag{15a}$$

$$|\psi_5\rangle \approx \left| \frac{3}{2} \right\rangle - \frac{\sqrt{18}\epsilon}{4\beta_E B} \left| \frac{-1}{2} \right\rangle \tag{15b}$$

$$|\psi_4\rangle \approx \left| \frac{1}{2} \right\rangle + \frac{\sqrt{10\epsilon}}{4\beta_E B} \left| \frac{5}{2} \right\rangle - \frac{\sqrt{18\epsilon}}{4\beta_E B} \left| \frac{-3}{2} \right\rangle \quad (15c)$$

$$|\psi_3\rangle \approx \left| \frac{-1}{2} \right\rangle - \frac{\sqrt{10\epsilon}}{4\beta_E B} \left| \frac{-5}{2} \right\rangle + \frac{\sqrt{18\epsilon}}{4\beta_E B} \left| \frac{3}{2} \right\rangle \quad (15d)$$

$$|\psi_2\rangle \approx \left| \frac{-3}{2} \right\rangle + \frac{\sqrt{18\epsilon}}{4\beta_E B} \left| \frac{1}{2} \right\rangle \quad (15e)$$

$$|\psi_1\rangle \approx \left| \frac{-5}{2} \right\rangle + \frac{\sqrt{10\epsilon}}{4\beta_E B} \left| \frac{-1}{2} \right\rangle \quad (15f)$$

These electron spin wavefunctions are then multiplied by the two nuclear spin wavefunctions $|I, m_I\rangle$. We can use $I=1/2$ in this calculation as quadrupole interactions are pure nuclear spin terms and are not affected by the electron-spin wavefunctions to first order. The first-order corrections in energies for the two lowest energy electron spin states substates ψ_1 and ψ_2 generated by \hat{H}_2 are then given as,

$$e^{(2)}(m_I) = \langle \psi_2 | S_Z | \psi_2 \rangle (m_I A_Y) - m_I \nu_N = \left(\frac{-3}{2} + 9(\Delta)^2 \right) (m_I A_Y) - m_I \nu_N \quad (16a)$$

$$e^{(1)}(m_I) = \langle \psi_1 | S_Z | \psi_1 \rangle (m_I A_Y) - m_I \nu_N = \left(\frac{-5}{2} - 5(\Delta)^2 \right) (m_I A_Y) - m_I \nu_N \quad (16b)$$

$$\Delta = \frac{\epsilon}{4\beta_E B} \quad (17)$$

where A_Y is the HFI constant projected along the Y -direction of the D -tensor and the parameter Δ incorporates the effect of the axial and rhombic contributions to the ZFS tensor on spectra taken along the ZFS Y axis. These energies in turn give the ENDOR transition frequencies, the absolute $\Delta m_I = \pm 1$ differences in energy for the two lowest energy electron-spin substates:

$$|\psi_2\rangle \quad \nu_+ = \left| -\frac{3}{2} A_Z - \nu_N + 9\Delta^2 A_Y \right| \quad (18a)$$

$$|\psi_1\rangle \quad \nu_- = \left| -\frac{5}{2} A_Z - \nu_N - 5\Delta^2 A_Y \right| \quad (18b)$$

In thus altering the wavefunctions and the two ENDOR frequencies associated with this sublevel EPR transition, the mixing thereby modifies both the splitting and center-frequency of the ENDOR doublet. As a result, Eq. (15) relate the

observed splitting, A_Y' , and the center-frequency of the doublet, ν_{av} , to the intrinsic HFI constant A_Y as modified by the correction factor Δ .

$$A_Y' = \left| A_Y(1 + 14\Delta^2) \right| \quad (19a)$$

$$\nu_{av} = 2|A_Y|(1 - \Delta^2) \quad (19b)$$

These expressions are analogous to those that describe the pseudo-nuclear Zeeman interactions that shifts the apparent nuclear Larmor frequency in ENDOR spectra of systems with $S > 1$ and large ZFS [21]. For Mn–D, with ZFS parameters $D = 7600$ MHz, $E/D = 0.15$ and an observed ^2H doublet splitting $A_Y' = -6$ MHz (Fig. 7), Eq. 17 gives a correction factor $\Delta = 0.108$ at 0.535 T. Use of Eqs. (18) and (19a) then yields the spin-Hamiltonian ^2H HFI constant, $A_Y = -5.2$ MHz and first-order-corrected ENDOR frequencies for the ^2H doublet, 3.7 and 9.7 MHz, which agree well with experiment, Fig. 7.

Finally, though the first-order Eq. (5) have the described limitations in the intermediate ZFS regime, they still offer utility in determining the sign of the effective hyperfine coupling when satellite electron-spin transitions (other than the $-1/2 \rightarrow 1/2$) are probed by ENDOR, such as the $-5/2 \rightarrow -3/2$ transition probed in the single-crystal-like ENDOR spectra of Fig. 7. For a measured doublet splitting with $|\Delta\nu|/\nu_N \lesssim 2$, as observed for the ^2H ENDOR spectra for Mn–D of Fig. 7, as shown in Fig. S6, if the coupling were positive the ENDOR doublet would be centered in the vicinity of $(4-5)\nu_N$; the observed centering at $\sim 2\nu_N$ instead unambiguously requires that the coupling $A_B' < 0$.

The perturbation-theory approach to the intermediate ZFS regime was corroborated by use of EasySpin calculations, which precisely gives the observed doubled center-frequency and splitting shift, as visualized in Fig. 8, where the experimental ENDOR spectrum of Mn–D at the low-field edge of the EPR spectrum (black trace) is compared to an EasySpin simulation (solid red trace), as well as to the expected frequencies if ZFS were negligible and Eq. (5) held true (dashed red trace). EasySpin simulations of measurements at other magnetic fields further gave the full ^2H hyperfine tensor used in these calculations. It is worth noting that the perpendicular component of the derived axial hyperfine tensor agrees well with A_Y obtained using the approach outlined above, and together they reveal that, as expected, the unique hyperfine coupling lies along D_z , which must lie along the Mn–D bond.

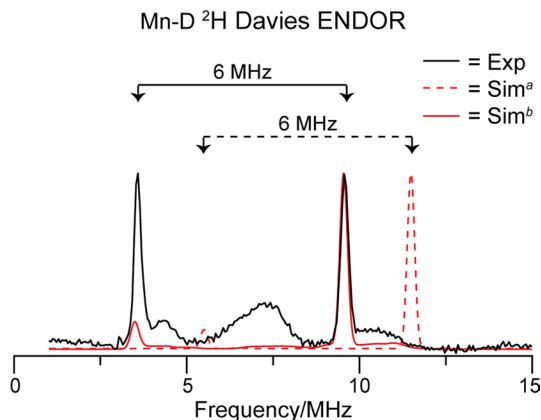


Fig. 8 Comparison between the experimentally observed ^2H Davies ENDOR (black trace) for Mn–D with simulation using EasySpin (red traces). Experimental spectrum is the same as Mn–D in Fig. 2. Simulation parameters for Sim^a (dashed red trace) are $S=5/2$; $g=2$; $A(^2\text{H})=-6$ MHz; negligible ZFS ($D=E=0$); temperature=0.5 K; microwave frequency=35 GHz; magnetic field=0.535 T; ENDOR linewidth=0.25 MHz; excitation width=300 MHz; Hstrain=250 MHz. Parameters for Sim^b (solid red trace) are the same as for Sim^a but with $D=[-1363, -3703, 5067]$ MHz; $A(^{55}\text{Mn})=-250$ MHz; $A(^2\text{H})=[-5.32, -5.32, 1.0]$ MHz, and temperature=2 K

5 Concluding Remark on the 80th Anniversary of the Discovery of EPR

The Mn^{2+} ion has been subjected to EPR measurement since the early days of EPR, and correspondingly for its ENDOR study. Thus, in celebration of the 80th anniversary of the invention of EPR, it seems fitting to offer a description of our ongoing efforts to build on past achievements.

Supplementary Information The online version contains supplementary material available at <https://doi.org/10.1007/s00723-024-01680-w>.

Acknowledgements This work was supported by the NIH (GM111097) and NSF (CHE2333907). We gratefully acknowledge the collaborators and their coworkers whose remarkable chemistry and biochemistry we had the good fortune to integrate with: (alphabetically) Judith P. Klinman; Alex McSkimming; Adam R. Offenbacher.

Author contributions All authors contributed to writing the main manuscript, P.E.D prepared figures 1, 2, 4, 5, A.S prepared figure 3, and A.D prepared figures 6, 7, 8.

Declarations

Conflict of interest The authors declare no conflicting/competing interests.

Ethical approval Not applicable.

References

1. R.L. McNaughton, A.R. Reddi, M.H. Clement, A. Sharma, K. Barnese, L. Rosenfeld, E.B. Gralla, J.S. Valentine, V.C. Culotta, B.M. Hoffman, Probing in vivo Mn²⁺ speciation and oxidative stress resistance in yeast cells with electron-nuclear double resonance spectroscopy. *Proc. Natl. Acad. Sci. USA* **107**(35), 15335–15339 (2010). <https://doi.org/10.1073/pnas.1009648107>
2. W.H. Horne, R.P. Volpe, G. Korza, S. DePratti, I.H. Conze, I. Shuryak, T. Grebenc, V.Y. Matrosova, E.K. Gaidamakova, R. Tkavc et al., Effects of desiccation and freezing on microbial ionizing radiation survivability: considerations for mars sample return. *Astrobiology* **22**(11), 1337–1350 (2022). <https://doi.org/10.1089/ast.2022.0065>
3. A. Sharma, C. Whittington, M. Javed, S.G. Hill, A. Kostenko, T. Yu, P. Li, P.E. Doan, B.M. Hoffman, A.R. Offenbacher, (13)C electron nuclear double resonance spectroscopy-guided molecular dynamics computations reveal the structure of the enzyme-substrate complex of an active, N-linked glycosylated lipoxygenase. *Biochemistry* **62**(10), 1531–1543 (2023). <https://doi.org/10.1021/acs.biochem.3c00119>
4. U.F. Lingappa, C.M. Yeager, A. Sharma, N.L. Lanza, D.P. Morales, G. Xie, A.D. Atencio, G.L. Chadwick, D.R. Monteverde, J.S. Magyar et al., An ecophysiological explanation for manganese enrichment in rock varnish. *Proc. Natl. Acad. Sci. USA* **118**(25), e2025188118 (2021). <https://doi.org/10.1073/pnas.2025188118>
5. M. Horitani, A.R. Offenbacher, C.A. Carr, T. Yu, V. Hoeke, G.E. Cutsail 3rd., S. Hammes-Schiffer, J.P. Klinman, B.M. Hoffman, (13)C ENDOR spectroscopy of lipoxygenase-substrate complexes reveals the structural basis for C-H activation by tunneling. *J. Am. Chem. Soc.* **139**(5), 1984–1997 (2017). <https://doi.org/10.1021/jacs.6b11856>
6. A.R. Offenbacher, A. Sharma, P.E. Doan, J.P. Klinman, B.M. Hoffman, The soybean lipoxygenase-substrate complex: correlation between the properties of tunneling-ready states and ENDOR-detected structures of ground states. *Biochemistry* **59**(7), 901–910 (2020). <https://doi.org/10.1021/acs.biochem.9b00861>
7. J. Telsner, Chapter Ten Paramagnetic resonance investigation of mono- and di-manganese-containing systems in biochemistry, in *Methods in Enzymology*, vol. 666, ed. by R.D. Britt (Academic Press, New York, 2022), pp.315–372
8. T.A. Stich, S. Lahiri, G. Yeagle, M. Dicus, M. Brynda, A. Gunn, C. Aznar, V.J. DeRose, R.D. Britt, Multifrequency pulsed EPR studies of biologically relevant manganese(II) complexes. *Appl. Magn. Reson.* **31**(1–2), 321–341 (2007)
9. A.V. Astashkin, A.M. Raitsimring, Electron spin echo envelope modulation theory for high electron spin systems in weak crystal field. *J. Chem. Phys.* **117**(13), 6121–6132 (2002). <https://doi.org/10.1063/1.1502651>
10. A.V. Astashkin, A.M. Raitsimring, P. Caravan, Pulsed ENDOR study of water coordination to Gd³⁺ complexes in orientationally disordered systems. *J. Phys. Chem. A* **108**(11), 1990–2001 (2004). <https://doi.org/10.1021/jp0307811>
11. S. Stoll, R.D. Britt, General and efficient simulation of pulse EPR spectra. *Phys. Chem. Chem. Phys.* **11**(31), 6614–6625 (2009). <https://doi.org/10.1039/B907277B>
12. M. Werst, C.E. Davoust, B.M. Hoffman, Ligand spin densities in blue copper proteins by q-band proton and nitrogen-14 ENDOR spectroscopy. *J. Am. Chem. Soc.* **113**(5), 1533–1538 (1991). <https://doi.org/10.1021/ja00005a011>
13. A. Schweiger, G. Jeschke, *Principles of Pulse Electron Paramagnetic Resonance* (Oxford University Press, Oxford, 2001)
14. B. Epel, I. Gromov, S. Stoll, A. Schweiger, D. Goldfarb, Spectrometer manager: A versatile control software for pulse EPR spectrometers. *Concept Magn. Reson. B* **26b**(1), 36–45 (2005). <https://doi.org/10.1002/cmr.b.20037>
15. B. Epel, D. Arieli, D. Baute, D. Goldfarb, Improving W-band pulsed ENDOR sensitivity—random acquisition and pulsed special TRIPLE. *J. Magn. Reson.* **164**(1), 78–83 (2003). [https://doi.org/10.1016/s1090-7807\(03\)00191-5](https://doi.org/10.1016/s1090-7807(03)00191-5)
16. S. Stoll, A. Schweiger, EasySpin, a comprehensive software package for spectral simulation and analysis in EPR. *J. Magn. Reson.* **178**(1), 42–55 (2006). <https://doi.org/10.1016/j.jmr.2005.08.013>
17. A. Drena, A. Fraker, N.B. Thompson, P.E. Doan, B. Hoffman, A. McSkimming, A terminal hydride complex of high-spin Mn. *JACS* (2024). <https://doi.org/10.1021/jacs.4c03310>

18. C. Whittington, A. Sharma, S.G. Hill, A.T. Iavarone, B.M. Hoffman, A.R. Offenbacher, Impact of N-glycosylation on protein structure and dynamics linked to enzymatic C-H activation in the *M. oryzae* lipoxygenase. *Biochemistry* **63**(10), 1335–1346 (2024). <https://doi.org/10.1021/acs.biochem.4c00109>
19. P.E. Doan, N.S. Lees, M. Shanmugam, B.M. Hoffman, Simulating suppression effects in pulsed ENDOR, and the “Hole in the Middle” of Mims and Davies ENDOR spectra. *Appl. Magn. Reson.* **37**(1–4), 763–779 (2010). <https://doi.org/10.1007/s00723-009-0083-6>
20. A.M. Raitsimring, A.V. Astashkin, O.G. Poluektov, P. Caravan, High-field pulsed EPR and ENDOR of Gd³⁺ complexes in glassy solutions. *Appl. Magn. Reson.* **28**(3), 281–295 (2005). <https://doi.org/10.1007/BF03166762>
21. A. Abragam, B. Bleaney, *Electron Paramagnetic Resonance of Transition Ions (International Series of Monographs on Physics)* (Clarendon, New York, 1970)

Publisher's Note Springer Nature remains neutral with regard to jurisdictional claims in published maps and institutional affiliations.

Springer Nature or its licensor (e.g. a society or other partner) holds exclusive rights to this article under a publishing agreement with the author(s) or other rightsholder(s); author self-archiving of the accepted manuscript version of this article is solely governed by the terms of such publishing agreement and applicable law.